Earth and Planetary Science Letters xxx (2011) xxx–xxx

Contents lists available at ScienceDirect

Earth and Planetary Science Letters

journal homepage: www.elsevier.com/locate/epsl

Solidus and liquidus profiles of chondritic mantle: Implication for melting of the Earth across its history

Denis Andrault [a,*], Nathalie Bolfan-Casanova [a], Giacomo Lo Nigro [a], Mohamed A. Bouhifd [a], Gaston Garbarino [b], Mohamed Mezouar [b]

[a] Laboratoire Magmas et Volcans, Université Blaise Pascal, Clermont-Ferrand, France
[b] European Synchrotron Radiation Facility, Grenoble, France

ARTICLE INFO

Article history:
Received 11 August 2010
Received in revised form 2 December 2010
Accepted 2 February 2011
Available online xxxx

Editor: L. Stixrude

Keywords:
lower-mantle melting-curves
properties of the magma ocean

ABSTRACT

We investigated the melting properties of a synthetic chondritic primitive mantle up to core–mantle boundary (CMB) pressures, using laser-heated diamond anvil cell. Melting criteria are essentially based on the use of X-rays provided by synchrotron radiation. We report a solidus melting curve lower than previously determined using optical methods. The liquidus curve is found between 300 and 600 K higher than the solidus over the entire lower mantle. At CMB pressures (135 GPa), the chondritic mantle solidus and liquidus reach 4150 (±150) K and 4725 (±150) K, respectively.

We discuss that the lower mantle is unlikely to melt in the D″-layer, except if the highest estimate of the temperature profile at the base of the mantle, which is associated with a very hot core, is confirmed. Therefore, recent suggestions of partial melting in the lowermost mantle based on seismic observations of ultra-low velocity zones indicate either (1) a outer core exceeding 4150 K at the CMB or (2) the presence of chemical heterogeneities with high concentration of fusible elements.

Our observations of a high liquidus temperature as well as a large gap between solidus and liquidus temperatures have important implications for the properties of the magma ocean during accretion. Not only complete melting of the lower mantle would require excessively high temperatures, but also, below liquidus temperatures partial melting should take place over a much larger depth interval than previously thought. In addition, magma adiabats suggest very high surface temperatures in case of a magma ocean that would extend to more than 40 GPa, as suggested by siderophile metal–silicate partitioning data. Such high surface temperature regime, where thermal blanketing is inefficient, points out to a transient character of the magma ocean, with a very fast cooling rate.

1. Introduction

A large proportion of our planet has experienced melting in the course of its accretion history as a consequence of the energy release associated with large impacts, radioactive decay and core formation. Major unknowns remain about this early time, in particular the extension depth of the magma ocean and the chemical signature inherited from mantle crystallization during cooling. The melting curve of the primitive mantle thus has major consequences for the existence of chemical heterogeneities and the survival of primitive mantle reservoirs. In the modern Earth, seismology evidences heterogeneous properties of the D″-region which extends from the core–mantle boundary (CMB) upwards 250 km (Lay et al., 1998). There are, indeed, evidences for large-scale patterns of heterogeneities, with anomalous set of V_P–V_S seismic velocities, that can hardly be explained by phase transitions in minerals or thermal anomalies. Instead, they seem to evidence chemical heterogeneities, which can be of different origins: (i) partial melting in the D″-layer (Lay et al., 2004), leading to chemical segregation of the mantle; (ii) relics of descending slabs rich in mid-ocean ridge basalts (MORB); (iii) zones enriched in incompatible elements associated to the progressive crystallization of an ancient magma ocean and trapped in the lowermost mantle (Labrosse et al., 2007); and/or (iv) lower mantle material affected by chemical exchanges with the outer core. Each hypothesis has specific implications for our comprehension of the dynamics of the Earth, as well as for elemental segregation between the different geological reservoirs. Unfortunately, it remains difficult to distinguish between the different scenarios. Indeed, the thermo-elastic parameters of the main lower mantle minerals are known with insufficient accuracy for inferring the mineralogy of this very remote region using the seismic features. Especially, it remains a challenge to infer any chemical anomaly other than Mg/Si and Fe/(Mg + Fe) ratios.

In order to assess the potential occurrence of partial melting in the D″ region, one must refine the melting curves of the different geological

* Corresponding author.
E-mail address: D.Andrault@opgc.univ-bpclermont.fr (D. Andrault).

0012-821X/$ – see front matter © 2011 Elsevier B.V. All rights reserved.
doi:10.1016/j.epsl.2011.02.006

materials. For pressures up to 25 GPa, melting curves of mantle silicates and phase relations in a partially molten mantle have been investigated using the multi-anvil press. It has been shown that pressure affects significantly the solidus and liquidus temperatures as well as composition of the eutectic liquids (Ito et al., 2004; Liebske et al., 2005; Litasov and Ohtani, 2002). At higher pressures, while the melting curve of end-member phases is relatively well documented using laser-heated diamond anvil cells (LH-DAC) (e.g. Boehler, 2000), shock wave experiments (e.g. Luo et al., 2004) or ab initio calculations (e.g. Stixrude and Karki, 2005), melting of material with relevant geological composition was much less investigated. For pyrolite, optical observations have been used to determine the melting curve as a function of pressure using the LH-DAC (Zerr et al., 1998), but only up to ~60 GPa. This pressure range remains too limited for quantitative extrapolation to the ~135 GPa representative of the D″-layer. On the other hand, using shock-wave experiments, melting of $(Mg, Fe)_2SiO_4$ olivine was reported at 4300 K and ~130 GPa (Holland and Ahrens, 1997). Recently, the same group corrected this value to 4000 (300) K, after improvement of the temperature estimation (Luo et al., 2004).

2. Methods

Ultra-brillant X-ray beams are now available from synchrotron rings for in-situ investigation of the melting behavior in the LH-DAC. For these experiments, we used a membrane-type DAC mounted with 250 μm or 75/300 μm culet-diameter diamonds. Re gaskets were pre-indented to 40 μm or 20 μm and laser-drilled to 80 μm or 50 μm, respectively. Small glass flakes were loaded in between two NaCl or KCl pellets, and a few experiments were performed without pressure medium. Salts provide good thermal insulation from the diamonds and can be used as pressure standards at 300 K (Sata et al., 2002; Walker et al., 2002). Hot spots with diameter larger than 30 μm were obtained by two YAG lasers aligned on both sides of the sample. Temperatures were measured from sample thermal emission using reflective lenses to prevent any chromatic aberration (Benedetti and Loubeyre, 2004). The intrinsic temperature uncertainty is estimated to be 50 K, including uncertainties on the thermal emissivity factors. For solid samples, temperature stability was better than 20 K during the 20 to 30 s of data acquisition. However, when the sample starts melting, the temperature stability deteriorates. In this study, we discarded those measurements where temperature fluctuation exceeded 50 K. Also, the emissivity factor is less documented for liquid phases. Therefore, the temperature uncertainty is estimated to be 50 K and 100 K, for solid and molten samples, respectively.

Our sample consisted of a synthetic CMASF glass with oxide contents in chondritic proportions (except for iron) so as to model the primitive mantle after core segregation (Wasson and Kallemeyn, 1988) (Table 1). We did not include minor and trace elements, which most abundant are Na (4900 ppm) and K (560 ppm). We believe that their effect on solidus and liquidus curves can be neglected as a first approximation because these elements are easily inserted in the $CaSiO_3$ perovskite phase (Ca–Pv) (Corgne et al., 2003). We did not mix our sample with any YAG-laser absorber or pressure standard, such as Pt or W, in order to avoid any chemical reaction. Finally, we estimate that the melting behavior of our starting material should be comparable to that of pyrolite, due to their related compositions (Ringwood, 1975) (Table 1).

Table 1
Composition of starting material used in this study, as measured by electron microprobe analyses. At lower mantle P–T conditions, the Ca–Pv, Mg–Pv, and Fp phase proportions are expected to be 4.5, 75.7, and 19.8 mol%, respectively. This composition is representative of a chondritic-type mantle (Wasson and Kallemeyn, 1988), and it is also quite close to pyrolite (Ringwood, 1975).

Oxide	Chondritic mantle (this study)		Pyrolite
	(wt.%)	(mol%)	(wt.%)
SiO_2	49.6	43.5	45.1
Al_2O_3	3.4	1.8	3.3
FeO	8.48	6.2	8.0
CaO	3.3	2.6	3.1
MgO	35.1	45.9	38.1

In order to probe the sample properties in-situ, we used the X-ray diffraction set-up available for LH-DAC at the ID27 beamline of ESRF (Mezouar et al., 2005). Wavelength was fixed to 0.3738 Å or 0.2647 Å. X-ray focusing to better than 2×3 μm^2 was achieved by two bent KB-mirrors. Typical acquisition time is 20–30 s using an imaging plate or a CCD detector. The X-ray beam position was determined from optical observations of the Re-gasket fluorescence. Therefore, combined images of X-ray beam and YAG lasers could be perfectly positioned on the pinhole of the entrance of the spectrometer used for temperature measurements. Integration of 2D-images and further data treatment were performed using the Fit2d and the GSAS packages, respectively.

For estimating pressure at high temperature, we used two different methods. The first one is based on the PVT equation of state (EoS) of $CaSiO_3$–perovskite (Shim et al., 2000) from which pressure is derived from the Ca–Pv volume at a known experimental temperature. Due to a non-negligible Al-solubility in Ca–Pv (Nishio-Hamane et al., 2007), its EoS could be affected, which would increase the experimental error. The second method is based on an estimation of the pressure correction (ΔP), which is a fraction of the theoretical thermal pressure (ΔP_{th}). The latter consists on an increase of pressure due to heating (ΔT) at constant volume, $\Delta P_{th} = \alpha K \Delta T$, where α and K are thermal expansion and bulk modulus, respectively. Experiments and calculations show that, due to partial volume relaxation at high-temperature, the effective ΔP corresponds to about half of the theoretical thermal pressure (Andrault et al., 1998). According to the thermo-elastic parameters of the main Mg–Pv component (Fiquet et al., 2000), the value of ΔP is $\sim 2.5 \cdot 10^{-3}$ GPa/K. Both methods give results similar within a couple of GPa. So, pressure error at high T is estimated to be about 3 GPa.

We investigated the melting temperature using NaCl and KCl as thermal insulators, but also tested without insulating pellets in a few experiments, in order to make sure that the results are not affected by the nature of the pressure transmitting medium. NaCl happens to melt at temperatures similar, or even below, the liquidus temperatures of the primitive chondritic mantle composition used. Therefore, all liquidus temperatures reported here were determined using KCl insulator. The data set presented in this paper includes 19 successful high-pressure loadings. Each melting point has been determined after laser-heating of at least one fresh piece of sample, i.e. melting at one single pressure.

3. Results

3.1. Melting criteria

In general, the onset of melting can be detected using X-ray diffraction by the appearance of a diffuse X-ray scattering band typical of liquids. Such band is easily observed if the sample is composed of relatively high-Z elements such as iron (Andrault et al., 2006; Shen et al., 2004). If the sample is composed of low Z-elements, such as is the case for a mantle silicate, the sample thickness should be important to enable observation of the diffuse band. This is not the case of our samples, which are intentionally thin in order to minimize axial thermal gradients.

Additional criteria based on X-ray observations are (1) the rapid re-crystallization of the sample at high-temperature, with appearance and disappearance of X-ray spots, indicative of coexistence of crystal and melt. (2) At the same time as solid and liquid coexist, the temperature reaches a plateau while laser power is continuously

Please cite this article as: Andrault, D., et al., Solidus and liquidus profiles of chondritic mantle: Implication for melting of the Earth across its history, Earth Planet. Sci. Lett. (2011), doi:10.1016/j.epsl.2011.02.006

increased, just before the liquid diffuse scattering appears and temperature simultaneously increases (Dewaele et al., 2007). In the following we used the fast disappearance of diffraction peaks of the solidus phase and re-crystallization as a sign of solidus temperature and the end of the temperature–power plateau as the sign of liquidus temperature.

3.2. Determination of solidus temperature

At sub-solidus temperatures, the phases present are $CaSiO_3$–perovskite (Ca–Pv), (Mg, Fe)O ferropericlase (Fp), and Al-bearing (Mg, Fe)SiO_3 perovskite (Mg–Pv), in the order of increasing abundance. The first phase to disappear from the diffraction patterns when increasing temperature is Ca–Pv (Fig. 1), in agreement with a previous study using multi-anvil press (Ito et al., 2004). Concerning Fp, persistence or disappearance of this phase is difficult to detect, first because its content is limited to 20 mol% for this chondritic-type composition and secondly because most of its diffraction lines overlap with those of Mg–Pv (Andrault, 2001). Thus, disappearance of Ca–Pv and Fp could be almost simultaneous. The Ca–Pv disappearance is concomitant with rapid grain growth of the Mg–Pv phase, as evidenced by larger diffraction spots on the diffraction image (Fig. 1A and B). Also, a number of diffraction peaks typical of the three phases reappear on the imaging plate after laser shut-down. Note that for such mineralogy, where at least three phases coexist, the kinetics of grain growth is extremely sluggish in the solid state (Yamazaki et al., 1996). Thus, changes of peak intensity can only be attributed to non-solid state diffusion, i.e. diffusion assisted by melt. Another source of information is based on the sample shape after laser-heating. In the case of heating to the solidus temperature, the shape of the sample is affected only moderately (Fig. 1D). Thermal expansion in the laser spot induced a circular-shaped structure, and some cracks in the surrounding material, at more than 10–15 μm from the center, where the material has not been heated at high temperatures. This shape contrasts largely with what is observed when heating to the liquidus temperatures (Fig. 2D).

We found that melting at the solidus temperature is very difficult to detect for those LH-DAC runs where we did not use any thermal insulator. The reason is that solidus melting is dispersed over a broad range of laser power, due to a large axial temperature gradient across the sample, given that the diamond remain basically cold compared to the center of the laser spot. Also, it is possible that a sample fraction remains below the solidus temperature at the diamond surface, before the central part of the sample reaches the liquidus temperature. Therefore, clear disappearance of $CaSiO_3$ (and/or Fp) diffraction lines cannot be observed in this case.

3.3. Determination of liquidus temperature

When approaching the liquidus temperature, we first observe a plateau where increasing laser power does not yield an increase

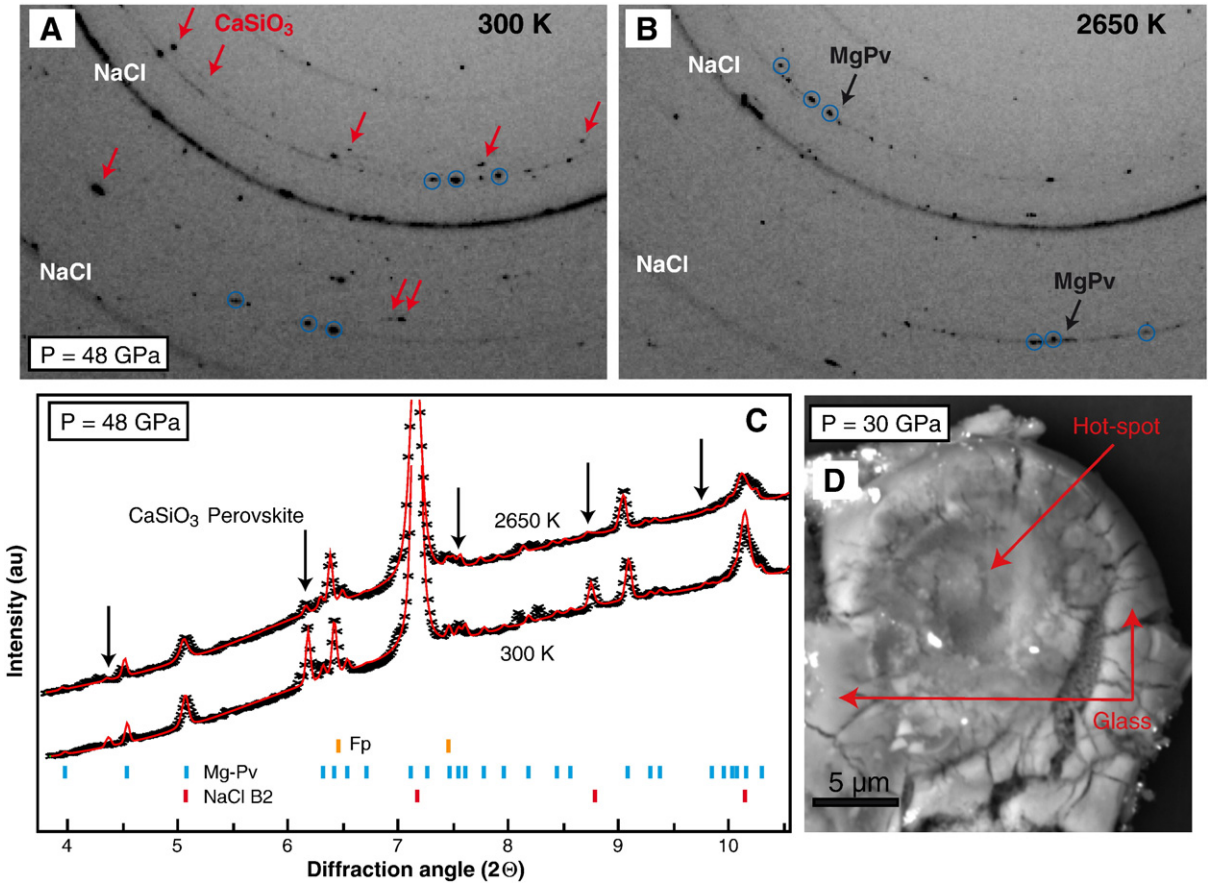

Fig. 1. Experimental evidences of sample partial melting and determination of the solidus temperature upon temperature increase from 300 K (A): at 2650 K (B) and a nominal pressure of 48 GPa, we observe first order changes in the position and intensity of diffraction peaks. First, disappearance of the $CaSiO_3$–perovskite diffraction peaks (pointed by arrows in (A) and (C)). Altogether, changes in peaks intensity are compatible with loss of 90% and 20% of the Ca-bearing and Mg-bearing perovskite phases, respectively. Simultaneously, we observe at 2650 K new spots of Mg–Pv phase (B) indicative of recrystallization on a short time scale, this can only be due to the presence of melt at grain boundaries. (D) Electron microphotograph showing a central zone of a sample recovered from 30 GPa that encountered laser heating between the solidus and liquidus temperatures (see Fig. 2D for comparison).

Please cite this article as: Andrault, D., et al., Solidus and liquidus profiles of chondritic mantle: Implication for melting of the Earth across its history, Earth Planet. Sci. Lett. (2011), doi:10.1016/j.epsl.2011.02.006

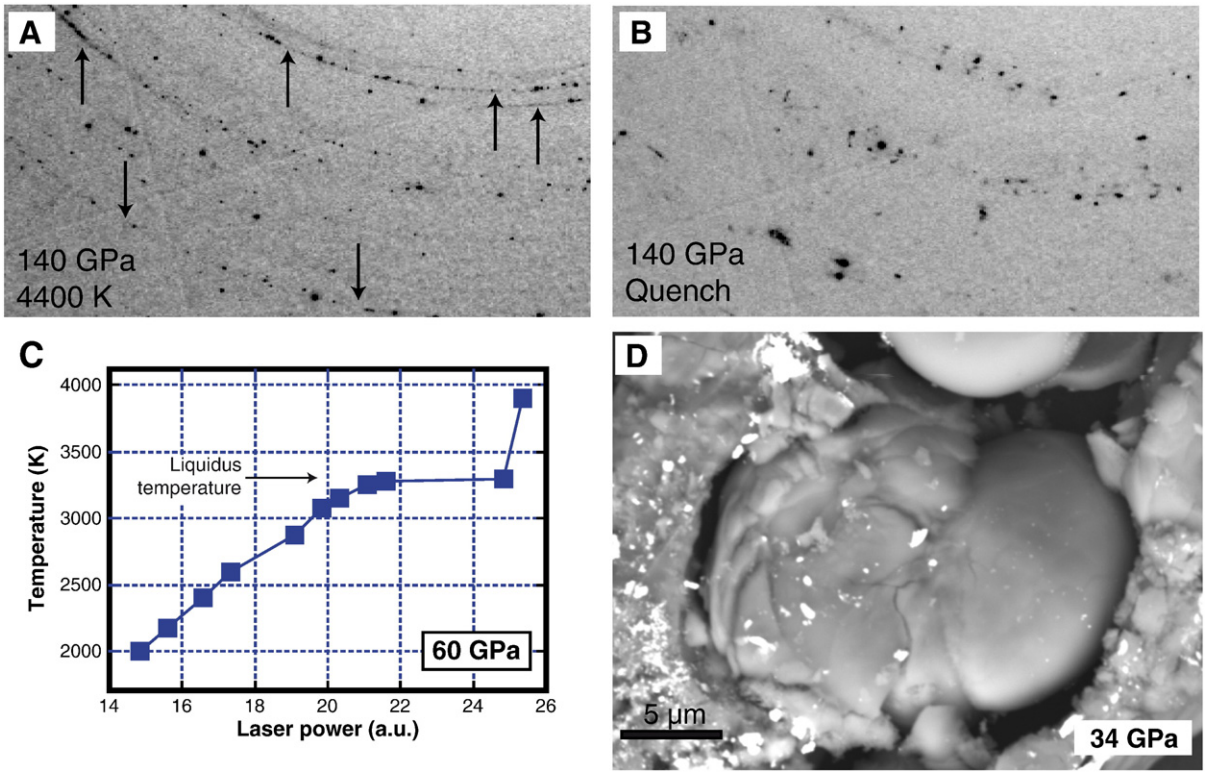

Fig. 2. Criterion used for determination of the liquidus temperature: X-ray diffraction pattern recorded (A) at 4400 K and (B) after quenching from 4800 K at a pressure of 140 GPa. Quench from the liquid phase (B) yields larger and new spots typical of sample recrystallization from a fully molten sample. Indeed, while these two diffraction patterns were taken a few minutes apart from each other, the patterns are radically different in peak positions and intensities. Also, we observe total disappearance of all fine and continuous diffraction lines (indicated by arrows in (A)), which evidences the complete melting of the Mg–Pv liquidus phase. (C) Sample temperature plotted as a function of the laser power. A discontinuity occurred at the liquidus temperature due to change in the absorption of the YAG-laser by the liquid sample. (D) Electron microphotograph of a sample recovered from 34 GPa showing the central laser-heated zone that underwent complete melting. It formed an independent liquid-ball separated from the rest of the sample.

in temperature, just before a sudden temperature jump of more than 500 K (Fig. 2C). A similar criterion has been used for melting determination in metals (Dewaele et al., 2007). We explain the plateau by a progressive disappearance of Mg–Pv with increasing laser power, with a coexisting liquid phase absorbing the YAG-radiation less than Mg–Pv. Indeed, a higher absorption efficiency for the solid is expected since Al-bearing (Mg, Fe)SiO_3 perovskite contains high Fe^{3+}-content (Lauterbach et al., 2000). The last data point on the plateau corresponds to the laser power required to finally achieve a good coupling between YAG-radiation and the silicate melt, i.e. once the phase that absorbs the YAG-radiation better (i.e. the Mg–Pv) is consumed. Moreover, the flatness of the plateau indicates that the melt fraction has no significant effect on melting temperature. Such a high liquid productivity is expected when incompatible elements are not abundant in the bulk composition, which clearly is our case, and when the liquid composition gets closer to the remaining solid phase, which is also our case for high degree of partial melting due to the fact that Mg–Pv, the liquidus phase, is very abundant in our samples (Asimow et al., 1997) (Table 1).

A very important feature is the total disappearance of the fine and continuous diffraction lines of the Mg–Pv phase in the high-temperature X-ray spectrum, evidencing that this phase is completely molten at that temperature (Fig. 2A). The diffuse X-ray scattering is not clearly visible in our samples because the sample is too thin. The reappearance of sparse and large diffraction spots upon temperature quench is typical of crystallization from a melt (Fig. 2B).

After quenching from the liquidus temperature, we observe a drastic change in the sample shape (Fig. 2D). The central part of the sample presents a round-shape with a diameter ~15–20 μm. This sample piece is detached from the rest of the sample. This part has undergone complete melting which induced deformation of the surrounding NaCl and KCl pressure medium to form a kind of sample droplet.

3.4. Melting curves

The solidus temperature is found to increase smoothly with pressure from ~2500 K to ~4200 K at 30 to 140 GPa. The liquidus is found at 300 to 600 K above the solidus (Fig. 3). Both melting curves are well fitted by modified Simon and Glatzel equation $[T = T_0\ (P/a+1)^{1/c}]$ with $T_0 = 2045$ K, $a = 92$ GPa and $c = 1.3$ for the solidus, $T_0 = 1940$ K, $a = 29$ GPa and $c = 1.9$ for the liquidus, where T_0 is the virtual (this mineral assemblage is only stable above 24 GPa) melting temperature at ambient pressure (Simon and Glatzel, 1929). The interpolation to the CMB pressure of 135 GPa yields solidus and liquidus temperatures of 4150 ± 150 K and 4725 ± 150 K, respectively. At low pressures, both solidus and liquidus curves are compatible with previous determinations using multi-anvil press (Litasov and Ohtani, 2002; Tronnes and Frost, 2002). Our liquidus curve falls between upper and lower bounds of the solidus curve reported previously using LH-DAC (Zerr et al., 1998). However, it is unlikely that the speckle method used by Zerr et al. can precisely determine solidus and liquidus temperature in the absence of in-situ X-ray diffraction observation. In addition, their melting curves must be shifted to higher pressures because they neglected the effect of thermal pressure inherent to the use of LH-DAC (~2.5 GPa/1000 K, see above). Such uncertainties, leading to overestimation of the melting temperature using optical methods, explain why the MORB melting curve of (Hirose et al., 1999) is observed at higher temperature than the solidus of our primitive mantle composition, although MORB is more fusible. Finally, the data point reported at 4300 K and ~125 GPa for melting of (Mg,

Please cite this article as: Andrault, D., et al., Solidus and liquidus profiles of chondritic mantle: Implication for melting of the Earth across its history, Earth Planet. Sci. Lett. (2011), doi:10.1016/j.epsl.2011.02.006

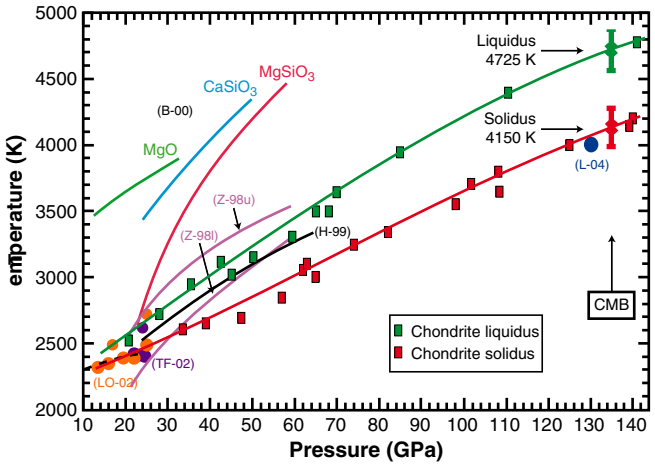

Fig. 3. Solidus (red squares) and liquidus (green squares) melting points and curve fits using the Simon–Glatzel model (continuous red and green lines) obtained for our chondritic-type mantle composition. These results are compared with previous works on the melting of lower mantle materials (Pyrolite: LO-02 (Litasov and Ohtani, 2002) and TF-02 (Tronnes and Frost, 2002) (full and open circle for solidus and liquidus, respectively) and Z-98 (Zerr et al., 1998) upper and lower estimations of the solidus; Mid-ocean ridge basalt: H-99 (Hirose et al., 1999); Olivine: L-04 (Luo et al., 2004); Simple oxides: B-00 (Boehler, 2000)). Melting criteria used in our experiments are described in Figs. 1 and 2. At the core–mantle boundary pressure of 135 GPa, we interpolate solidus and liquidus melting temperatures at 4150 K and 4725 K, respectively. Error bars for all points are shown at CMB pressures. (For interpretation of the references to color in this figure legend, the reader is referred to the web version of this article.)

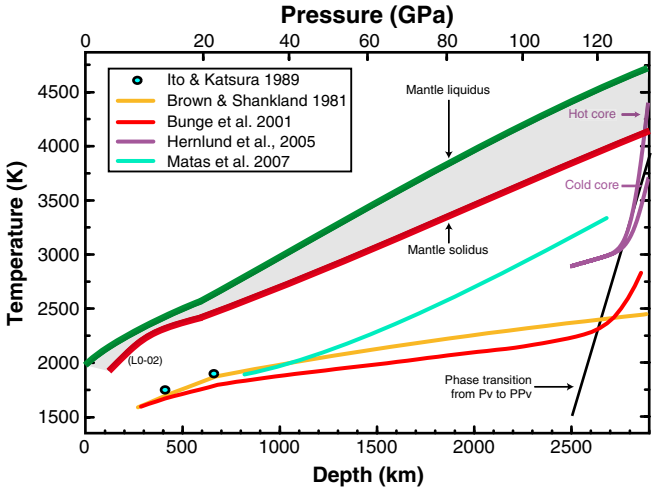

Fig. 4. The melting curves of synthetic chondritic mantle plotted together with available estimates of the mantle geotherm (Brown and Shankland, 1981; Bunge et al., 2001; Hernlund et al., 2005; Matas et al., 2007) and temperature anchor points (Ito and Katsura, 1989). Although the temperature estimates vary significantly from one work to another, there is only one estimate for the D″-layer temperatures (Hernlund et al., 2005) being higher than the experimentally determined melting curve for chondritic mantle. It is based on the double-crossing of the $MgSiO_3$ Pv to Post-Pv phase transition and remains controversial (see text).

$Fe)_2SiO_4$ olivine from shock-experiments (Holland and Ahrens, 1997) falls in between our solidus and liquidus melting curves, showing a relatively good agreement between the two different data sets. Indeed the forsterite liquidus is observed to be lower than that of enstatite at high-pressures (Mosenfelder et al., 2009).

4. Discussions

4.1. Thermal structure of the D″ layer

In order to identify melting in the mantle, melting curves must be compared to the geotherm. While temperatures are relatively well constrained in the shallow mantle due to anchoring by phase transitions at 410 and 670 km depth in (Mg, $Fe)_2SiO_4$ (Ito and Katsura, 1989), extrapolation of the adiabatic geotherm ($dT/dz = \alpha gT/Cp$, where α, g, Cp are thermal expansion, gravity and heat capacity at constant pressure) to the base of the mantle using the elastic parameters of constitutive mantle minerals bears a much larger uncertainty (Fig. 4). Differences in adiabatic geotherms are often within 0.1 K/km but translate into up to 250 K difference at the bottom of the mantle yielding in general 2500 K ± 250 at 2700 km depth (Brown and Shankland, 1981; Bunge et al., 2001; Stacey and Davis, 2004). Whereas more sophisticated models using inversion of seismic radial profiles indicate hotter temperatures of 2800 to 3400 K at 2700 km depth (Matas et al., 2007), dependent on the Mg/Si ratio.

The temperature profile in the D″-layer could be much steeper accounting for the difference in temperature between the mean mantle above and the molten outer core. The present-time temperature gradient in this zone depends on the initial difference in temperature between the outer core and the mantle a few hundreds kilometers above the CMB, the core energy budget since its formation (Labrosse et al., 1997), the thickness of the boundary layer and the thermal conductivities. Recently, the thermal structure of the D″ region has been tentatively constrained in light of the new post-perovskite phase of $MgSiO_3$ (Murakami et al., 2004; Oganov and Ono, 2004). It was proposed that the observation of pairs of positive and negative S-wave velocity jumps in the D″ region are due to double-crossing of the perovskite to post-perovskite (PPv) transition (Hernlund et al., 2005). Based on the latest measurements of the Pv-PPv Clapeyron slope in $MgSiO_3$, this would mean that the temperature at the CMB could be around 3700 K (Tateno et al., 2009). Still, it can be argued that the lower mantle contains Fe and Al that are known to influence the depth and thickness of phase transitions in general and have been demonstrated recently to considerably broaden the Pv−PPv transition due to the very different iron partitioning between the two phases (Andrault et al., 2010; Catalli et al., 2009). The interpretation of the seismic discontinuities in terms of temperature should thus be revised in order to take this into account.

In any case, refining the outer core temperature remains essential for our knowledge of the temperature profile in the D″-layer. This temperature is generally estimated by extrapolating the adiabatic temperature profile from the inner-core boundary (ICB) through the outer core. However, there are several sources of uncertainties. A first uncertainty arises from controversial melting curves for pure Fe determined firstly by LHDAC, ranging from 4850 ± 200 K (Boehler, 1993) to 7600 ± 500 K (Williams et al., 1987) at ICB pressures. On the other hand, shock-wave experiments and ab-initio calculations suggest melting temperatures of more than 6000 K at 330 GPa (Alfe, 2009; Nguyen and Holmes, 2004). A second source of uncertainty is associated to the presence and nature of light elements, which should cause a severe melting temperature depletion. Depending on the major light element considered for the outer core, extrapolations of the melting temperature to the ICB yields temperatures from 4100 ± 100 K in the Fe−Si system (Asanuma et al., 2010) to 5500 ± 500 K in the Fe−S eutectic system (Kamada et al., 2010), for example. And, if the outer core contains a mixture of light elements S, Si and O (Badro et al., 2007; Poirier, 1994), the resulting melting temperature should be lower than measured in binary compounds. Altogether, the broad range of ICB temperatures reported in the literature yields a large range of CMB temperatures and it is difficult to conclude if the outer core is indeed much hotter than the lower mantle at a few hundreds kilometers above the CMB or not.

4.2. Melting in the D″ region and origin of the ULVZ

From the available geotherms, only the highest temperature estimation, based on an extremely steep temperature gradient in

Please cite this article as: Andrault, D., et al., Solidus and liquidus profiles of chondritic mantle: Implication for melting of the Earth across its history, Earth Planet. Sci. Lett. (2011), doi:10.1016/j.epsl.2011.02.006

the D″-layer allows partial melting of a chondritic-type mantle in the D″-layer for which we report a solidus temperature of 4150 K (Fig. 4). However, we insist on the fact that this very steep temperature profile is derived from the Clapeyron slope of the Pv—PPv transition for pure $MgSiO_3$ (Hernlund et al., 2005), and that in the mantle the transition does not occur at the same depths. Therefore, if partial melting of the chondritic (or pyrolitic) lower mantle is not totally precluded in the D″-layer, it remains unlikely as long as the occurrence of a very hot core is not better established.

The observation of ultra-low velocity zones (ULVZ) exhibiting P- and S-wave velocity reductions of 10 and 30% just above the CMB (Lay et al., 2004) has been interpreted as being the result of partial melting. Since the solidus and liquidus profiles determined in this study are not in favor of partial melting of the chondritic (or pyrolitic) mantle, a probable way for inducing melting in the ULVZ of the D″-layer is a local enrichment in incompatible elements, in particular volatiles (Na, K, H or CO_2) which are known to depress the solidus temperatures. Some of these elements (Na and K) may have a moderate effect on the solidus temperature, since they are easily inserted into the Ca-Pv at sub-solidus conditions (Corgne et al., 2003). In the case of water, however, the effect could be large, because the solubility of H in the main lower mantle phases is low (Bolfan-Casanova et al., 2006). Once partial melting is induced, the degree of partial melting is difficult to estimate since solid–liquid phase relations are basically unknown at CMB conditions. Local concentration of the most fusible elements associated with chemical heterogeneities is compatible with the fact that ULVZ features are not ubiquitous but instead observed only in one third of investigated areas (Wen and Helmberger, 1998).

4.3. Depth extension of the early magma ocean

The energy deposited on the Earth during its accretion was sufficient to partially or completely melt it, especially just after the Moon-forming giant impact (Canup, 2008; Tonks and Melosh, 1993). Under such conditions, a magma ocean undoubtedly existed. It is interesting to discuss the implications of the new melting curve of chondritic mantle for our understanding of the nature of the magma ocean.

The inventory of siderophile elements in the modern mantle indicates equilibration between silicates and iron at high pressures and temperatures (Li and Agee, 1996; Righter et al., 1997). In addition, in order to efficiently segregate the core, the silicate has to be molten in order to overcome the high surface tension of iron in a solid silicate matrix. Consequently, it was proposed that iron droplets sink through the molten silicate layer and pond at the base of a magma ocean, followed by metal descending through the solid mantle in the form of diapirs (Karato and Murthy, 1997; Stevenson, 1990). Thus, a widely accepted model is that equilibration occurred just before the iron droplets reach the Fe-pond at the floor of a magma ocean (Li and Agee, 1996; Wood et al., 2006). The apparent pressure of equilibrium is comprised between 30 and 60 GPa, 45 and 85 GPa, or 20 and 50 GPa, based on metal–silicate partition coefficients of nickel and cobalt (Bouhifd and Jephcoat, 2003; Chabot et al., 2005), oxygen solubility in molten iron (Rubie et al., 2004), or metal–silicate partitioning of tungsten (Cottrell et al., 2009), respectively. A recent refinement of such model explains the mantle enrichment in several siderophile elements by a continuous accretion at a pressure of equilibrium of 40 GPa and 3150 K (Wood et al., 2006). The pressure of equilibrium is given by the partitioning of Ni and Co that is very sensitive to pressure while the temperature of equilibrium is estimated from the partitioning of V which is very sensitive to temperature. However, complications may arise from the fact that diffusion kinetics suggest metal–silicate equilibration during a “metal rainfall” so that the resulting chemical composition of the mantle probably results from a polybaric process (Rubie et al., 2003), extending the pressure range of equilibrium to depths shallower than the base of the magma ocean.

We should also mention here that the model of equilibrium core segregation is challenged by numerical modeling results indicating that the core of the impactors possibly merged with the Earth's core or that the impact did not emulsify efficiently the metal and silicate liquids (Dahl and Stevenson, 2010). Both imply that the core segregated without equilibrating with the mantle. In this case, the pressure of equilibration is meaningless. Still, the geochemical constraints (Hf–W, U–Pb, and siderophile elements) do not seem to be enough in order to conclude whether the core and mantle fully or partly equilibrated. It seems that the siderophile pattern of the mantle can be reproduced under non-equilibrium conditions assuming oxygen fugacity conditions higher than previously thought and embryos that have equilibrated at excessively high-temperatures (450 K above liquidus of chondritic mantle) (Rudge et al., 2010). In the following, since the disequilibrium core formation model creates more questions than answers, we will assume equilibrium core–mantle segregation at 45–50 GPa in agreement with metal–silicate partitioning experiments.

We report in Fig. 5 liquidus and solidus curves measured for a chondritic mantle superimposed with the adiabats for the liquid (Mosenfelder et al., 2009; Stixrude and Karki, 2005). Here we focus on isentropes calculated by Mosenfelder et al. (2009), based on their latest shock-wave equation of state (Eos) of molten $MgSiO_3$. Such liquid is comparable to the chondritic mantle composition used in this study that contains ~70 mol% $MgSiO_3$ end-member. In the classical model of equilibrium at the base of a magma ocean, it is implicitly assumed that equilibrium occurs at 45–50 GPa on the liquidus (e.g. (Wood et al., 2006)). According to our measurements of the liquidus, a fully molten chondritic mantle that would extend to a pressure of 45–50 (±10) GPa exhibits a temperature of ~3175 K (±250 K) at a depth of ~1175 (±250) km. Such conditions correspond to a surface potential temperature of 2450 K (±150 K) (See red curves in Fig. 5). Such a hot surface is not stable and is only compatible with a transient magma ocean. Indeed, it has been demonstrated that surface temperatures significantly higher than 1700–1800 K prevent formation of an (H_2O–CO_2)-rich atmosphere required to produce an efficient thermal blanket to the magma ocean. Without such blanketing the magma ocean will cool down very rapidly (Abe and

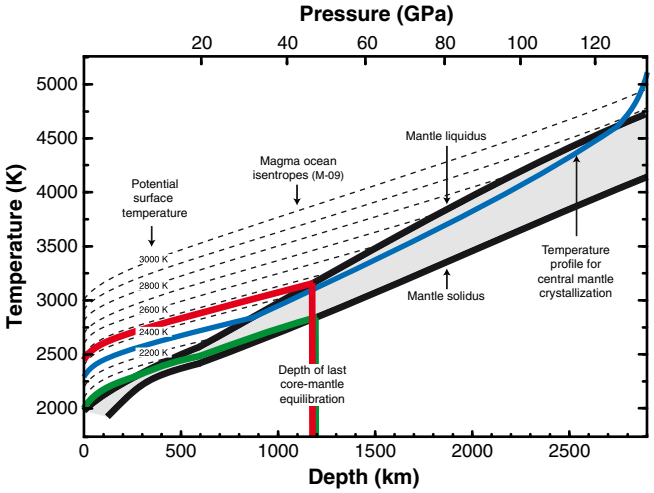

Fig. 5. The melting curves of synthetic chondritic mantle plotted together with isentropic temperature profiles of the magma ocean calculated for different potential surface temperatures (Mosenfelder et al., 2009). Metal–silicate partitioning coefficients determined experimentally evidence that core–mantle segregation occurred at a depth of ~1175 (±250) km. Such depth corresponds to a surface temperature of ~2000 K (green line) or 2450 K (red line) if this limit corresponds to solidus or liquidus temperature of the magma ocean, respectively. On the other hand, we propose a possible mantle geotherm (blue line) compatible with crystallization of the liquidus phase Mg–Pv at the center of the mantle. (For interpretation of the references to color in this figure legend, the reader is referred to the web version of this article.)

Please cite this article as: Andrault, D., et al., Solidus and liquidus profiles of chondritic mantle: Implication for melting of the Earth across its history, Earth Planet. Sci. Lett. (2011), doi:10.1016/j.epsl.2011.02.006

Matsui, 1988; Zahnle et al., 1988). Indeed, above 1700–1800 K significant silicate vaporization occurs (Nagahara and Ozawa, 1996) and such rock vapor atmosphere conducts heat easily so that the magma ocean would cool down in a few thousand years, before the magma ocean surface temperature comes back to 1700–1800 K (Sleep et al., 2001). Note that only shallow magma oceans (shallower than 5 GPa) are consistent with surface temperatures of 1700–1800 K (Miller et al., 1991, see their Figure 8) and can survive for long periods.

On the other hand, Hf–W chronology indicates that ~80% of the core formed within the first 30 million years of the Earth's history (Kleine et al., 2002). As discussed above, deep magma ocean extending to 45–50 GPa pressure can only last for a few thousand years, and such time scale is radically different from that inferred from Hf–W isotopes. Thus, one must refine the scenario of core–mantle segregation in order to explain these apparent contradictions:

(a) If the metal droplets do not rain faster than the crystallization rate of the hot (transient) magma ocean (Rubie et al., 2003; Solomatov, 2000), they fall in the liquid mantle to intermediate depth until the silicate phases crystallize. Then, the metal remains embedded in the solid mantle until the next melting event. We note here that the descent of iron droplets is intrinsically associated with heat production by release of gravitational energy. Thus, in order to stop the Fe rain, the heat flux at the Earth's surface should be higher than the gravitational energy release. The droplet can also descend slowly by percolative flow (Yoshino et al., 2003). In this scenario (Fig. 6A), the equilibrium pressure of 45–50 GPa corresponds to the mean extension depth of the last magma ocean before the Fe droplets coalence into larger diapirs and fall into the core.

(b) A second possible scenario involves a magma ocean defined by its solidus located at ~1175 km depth (45–50 GPa) (Fig. 6B). From the base of this magma ocean upwards, coexistence of solid and melt is expected to occur over a broad depth interval due (i) to the large temperature difference between solidus and liquidus (Fig. 5) and (ii) to the fact that the adiabats of partially molten mantle are sub-parallel to the liquidus (Miller et al., 1991). It follows that this magma ocean is on its liquidus at depth close to 300–400 km. As a consequence, the melt adiabats indicate a surface temperature approaching 2000 K, compatible with a blanketed magma ocean, which would thus cool down slowly. In this situation, the metal rains and equilibrates in a mush rather than in a completely molten magma ocean.

4.4. Formation of a basal magma ocean?

Finally, our new melting curve can be used to discuss the possible existence of an ancient magma ocean starting its crystallization in the mid-lower mantle, with formation of a basal magma ocean (Labrosse et al., 2007). First, we should note that complete melting of the Earth mantle implies a surface temperature higher than 2800 K (Fig. 5), which is much above the vaporization temperature of the silicate mantle (Nagahara and Ozawa, 1996). Thus, cooling and crystallization of the mantle should occur very quickly, as discussed in the previous paragraph. In addition, this scenario implies temperatures higher than the liquidus in both the shallow and lowermost mantle, and temperatures becoming lower than the liquidus at intermediate depth due to secular cooling. Such a temperature profile requires a very hot core in order to induce a geotherm steeper than the liquidus in the lowermost mantle (see blue curve in Fig. 5). However, such temperature gradient is unlikely to be relevant to the primitive Earth for a long time. High thermal conductivities expected for both the liquid in the D″-layer and the partial melt at mid mantle depth should help to propagate heat from the CMB to shallower mantle depth and resolve a potential steep temperature gradient in the lowermost mantle. Therefore, it appears unlikely that the outer core temperature could exceed 4725 K at the CMB after crystallization of the magma ocean.

In the context of a complete (or almost complete) melting of the mantle, it is unlikely that the temperature profile could reach the solidus in the mid-lower mantle given (i) the large temperature difference found between solidus and liquidus temperatures; (ii) the fact that the solidus and liquidus are almost straight curves that remain steep at CMB conditions; and (iii) because the isentropes of partially molten mantle are steeper than melt adiabats (Fig. 5). Due to the later effect, it was argued that the partially molten mantle could extend up to the core mantle boundary when the depth of a completely molten mantle extends to a pressure of more than 40 GPa (Kojitani and Akaogi, 1997; Miller et al., 1991; Stixrude et al., 2009). Therefore, the mantle fraction defined as “solid mantle” by (Labrosse

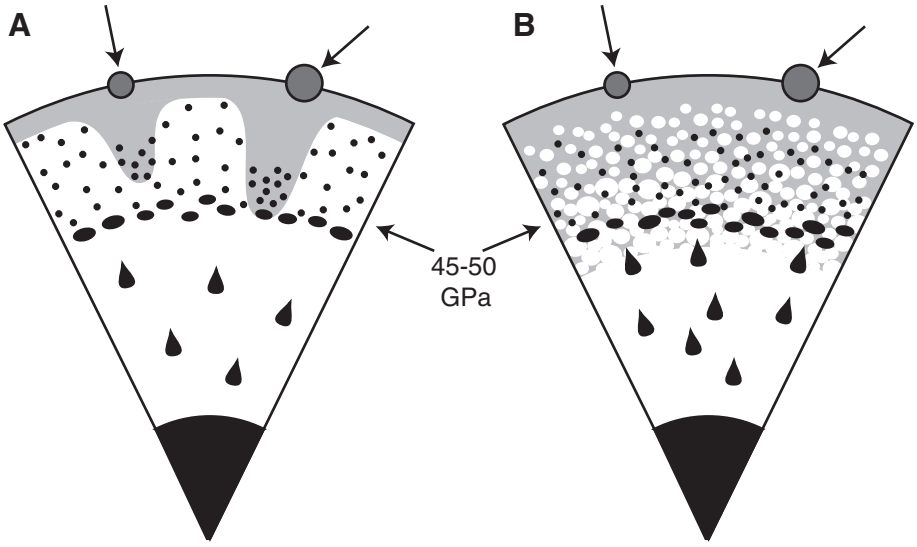

Fig. 6. Models for core–mantle segregation that respect (i) an equilibrium pressure of 45–50 GPa as suggested by metal–silicate partitioning experiments and (ii) a shallow completely molten magma ocean that can be compatible with a moderate surface temperature. In model (A) representative of transient magma oceans cooling very fast, the metal droplets remain embedded in the solid mantle and their progression to greater depths is aided by successive melting events. In model (B) representative of a sustained magma ocean cooling slowly, metal droplets fall in a partially molten mantle until the fraction of solid mantle becomes too high, at temperatures close to the solidus.

Please cite this article as: Andrault, D., et al., Solidus and liquidus profiles of chondritic mantle: Implication for melting of the Earth across its history, Earth Planet. Sci. Lett. (2011), doi:10.1016/j.epsl.2011.02.006

et al., 2007) could only correspond to a partially crystallized mantle, where the solid phase would essentially be the liquidus phase i.e. Mg–Pv (Fig. 1 and (Ito et al., 2004)). If crystallization of the magma ocean from the middle is associated to formation of a perovskitic layer, geochemical arguments constrain it to be at most 13% of the whole mantle, a minimum for which the upper mantle refractory elements budget still remains chondritic (Liebske et al., 2005).

Alternatively, a basal magma ocean could be possible if its composition is enriched in incompatible (i.e. fusible) elements, which would facilitate melting at lower temperatures at the base of the mantle. The persistence of such fusible material until today would be compatible with the observation of ULVZ, as mentioned in a previous paragraph. It could also explain major geochemical signatures, such as the one associated to "primitive mantle" with high ^{3}He, for example (Allègre et al., 1995; Kurz et al., 1982).

5. Conclusions

We have determined the solidus and liquidus curves of a chondritic mantle up to CMB pressures. Our melting criteria include in-situ X-ray diffraction and temperature–power relationships. We confirm that the $MgSiO_3$-bearing perovskite is the liquidus phase in the deep lower mantle. The solidus melting curve is found at lower temperature than reported previously, especially at mid-lower mantle depth, while the liquidus is found at significantly higher temperatures at all mantle depths. At the CMB, we report solidus and liquidus melting at 4150 ± 150 K and 4725 ± 150 K, respectively.

We then discussed the geophysical implications of the new melting curve for chondritic mantle. First, it appears unlikely that the ULVZ, which is interpreted to experience ~20% partial melting, is of chondritic (or pyrolitic) composition. Indeed, the solidus of 4150 ± 150 K appears to be too high compared to estimates of the temperature profile in the D″ region, except if the core is extremely hot. Thus, in order to be explained by melting the ULVZ should rather be associated to high concentration of fusible elements that decrease the melting point compared to the chondritic mantle.

We also show that the pressure of 45–50 GPa typical of metal–silicate equilibrium, as reported by several experimental studies in the context of core–mantle segregation, is associated to a magma ocean surface temperature incompatible with a sustained magma ocean. It strongly suggests that the metal–silicate equilibrium occurred in a partially molten mantle, covered by a fully molten magma ocean much thinner than 1000 km.

Finally, by examining the relationships between magma ocean temperatures at depth and potential surface temperatures, our melting diagram is compatible with the formation of a basal magma ocean only if the middle-depth solid mantle is mainly composed of Al-bearing $(Mg, Fe)SiO_3$-perovskite and if the basal magma ocean has a chemical composition significantly different than the chondritic mantle.

Acknowledgments

We thank N. Guignot, T. Hammouda, J.P. Perrillat and S. Petitgirard for participation to some experiments, S. Labrosse and H. Martin for fruitful discussions, and Paul Asimow for a fruitful review. This work is supported by Région Auvergne, INSU-CNRS, FEDER and the European C2C program.

References

Abe, Y., Matsui, T., 1988. Evolution of an impact-generated H_2O–CO_2 atmosphere and formation of a hot proto-ocean on Earth. J. Atmos. Sci. 45, 3081–3101.
Alfe, D., 2009. Temperature of the inner-core boundary of the Earth: melting of iron at high pressure from first-principles coexistence simulations. Phys. Rev. B 79.
Allègre, C.J., Moreira, M., Staudacher, T., 1995. ^{4}He/^{3}He dispersion and mantle convection. Geophys. Res. Lett. 22, 2325–2328.
Andrault, D., 2001. Evaluation of (Mg, Fe) partitioning between perovskite and magnesiowustite up to 120 GPa. J. Geophys. Res. 106, 2079–2087.
Andrault, D., Fiquet, G., Itié, J.P., Richet, P., Gillet, P., Häusermann, D., Hanfland, M., 1998. Thermal pressure in a laser-heated diamond-anvil cell: an X-ray diffraction study. Eur. J. Mineral. 10, 931–940.
Andrault, D., Morard, G., Bolfan-Casanova, N., Ohtaka, O., Fukui, H., Arima, H., Guignot, N., Funakoshi, K., Lazor, P., Mezouar, M., 2006. Study of partial melting at high pressure using *in situ* X-ray diffraction. High Pressure Res. 26, 267–276.
Andrault, D., Munoz, M., Bolfan-Casanova, N., Guignot, N., Perrillat, J.P., Aquilanti, G., Pascarelli, S., 2010. Experimental evidence for perovskite and post-perovskite coexistence throughout the whole D″ region. Earth Planet. Sci. 293, 90–96.
Asanuma, H., Ohtani, E., Sakai, T., Terasaki, H., Kamada, S., Kondo, T., Kikegawa, T., 2010. Melting of iron–silicon alloy up to the core–mantle boundary pressure: implications to the thermal structure of the Earth's core. Phys. Chem. Miner. 37, 353–359.
Asimow, P.D., Hirschmann, M.M., Stolper, E.M., 1997. An analysis of variations in isentropic melt productivity. Philos. Trans. R. Soc. Lond. 355, 255–281.
Badro, J., Fiquet, G., Guyot, F., Gregoryanz, E., Occelli, F., Antonangeli, D., d'Astuto, M., 2007. Effect of light elements on the sound velocities in solid iron: implications for the composition of Earth's core. Earth Planet. Sci. 254, 233–238.
Benedetti, R., Loubeyre, P., 2004. Temperature gradients, wavelength-dependent emissivity, and accuracy of high and very-high temperatures measured in the laser heated diamond anvil cell. High Pressure Res. 24, 423–445.
Boehler, R., 1993. Temperatures in the Earth's core from melting-point measurements of iron at high static pressures. Nature 363, 534–536.
Boehler, R., 2000. High-pressure experiments and the phase diagram of lower mantle and core materials. Rev. Geophys. 38, 221–245.
Bolfan-Casanova, N., McCammon, C.A., Mackwell, S., 2006. Water in the transition zone and lower mantle minerals. In: Jacobsen, S.J., van der Lee, S. (Eds.), The Earth's Deep Water Cycle: Geophysical Monographs, AGU, pp. 57–68.
Bouhifd, M.A., Jephcoat, A.P., 2003. The effect of pressure on partitioning of Ni and Co between silicate and iron-rich metal liquids: a diamond anvil cell study. Earth Planet. Sci. 209, 245–255.
Brown, J.M., Shankland, T., 1981. Thermodynamic parameters in the Earth as determined from seismic profiles. Geophys. J. R. Astron. Soc. 66, 579–596.
Bunge, H.P., Ricard, Y., Matas, J., 2001. Non-adiabaticity in mantle convection. Geophys. Res. Lett. 28, 879–882.
Canup, R.M., 2008. Accretion of the Earth. Phil. Trans. R. Soc. A 366, 4061–4075.
Catalli, K., Shim, S.H., Prakapenka, V.B., 2009. Thickness and Clarpyron slope of the post-perovskite boundary. Nature 462, 782–785.
Chabot, N.L., Draper, D.S., Agee, C.B., 2005. Conditions of core formation in the Earth: constraints from nickel and cobalt partitioning. Geochim. Cosmochim. Acta 69, 2141–2151.
Corgne, A., Allan, N.L., Wood, B.J., 2003. Atomistic simulations of trace element incorporation into the large site of $MgSiO_3$ and $CaSiO_3$ perovskites. Phys. Earth Planet. Inter. 139, 113–127.
Cottrell, E., Walter, M.J., Walker, D., 2009. Metal–silicate partitioning of tungsten at high pressure and temperature: implications for equilibrium core formation in Earth. Earth Planet. Sci. 281, 275–287.
Dahl, T.W., Stevenson, D.J., 2010. Turbulent mixing of metal and silicate during planet accretion- and interpretation of the Hf–W chronometer. Earth Planet. Sci. 295, 177–186.
Dewaele, A., Mezouar, M., Guignot, N., Loubeyre, P., 2007. Melting of lead under high pressure studied using second-scale time-resolved X-ray diffraction. Phys. Rev. B 76, 144106.
Fiquet, G., Dewaele, A., Andrault, D., Kunz, M., Le Bihan, T., 2000. Thermoelastic properties and crystal structure of $MgSiO_3$ perovskite at lower mantle pressure and temperature conditions. Geophys. Res. Lett. 27, 21–24.
Hernlund, J.W., Thomas, C., Tackley, P.J., 2005. A doubling of the post-perovskite phase boundary and structure of the Earth's lowermost mantle. Nature 434, 882–886.
Hirose, K., Fei, Y., Ma, P., Mao, H.K., 1999. The fate of subducted basaltic crust in the Earth's lower mantle. Nature 397, 53–56.
Holland, K.G., Ahrens, T.J., 1997. Melting of (Mg, Fe)2SiO4 at the core–mantle boundary of the Earth. Science 275, 1623–1625.
Ito, E., Katsura, T., 1989. A temperature profile for the mantle transition zone. Geophys. Res. Lett. 16, 425–428.
Ito, E., Kubo, A., Katsura, T., Walter, M.J., 2004. Melting experiments of mantle materials under lower mantle conditions with implications for magma ocean differentiation. Phys. Earth Planet. Inter. 143–144, 397–406.
Kamada, S., Terasaki, H., Ohtani, E., Sakai, T., Kikegawa, T., Ohishi, Y., Hirao, N., Sata, N., Kondo, T., 2010. Phase relationships of the Fe–FeS system in conditions up to the Earth's outer core. Earth Planet. Sci. 294, 94–100.
Karato, S., Murthy, V.R., 1997. Core formation and chemical equilibrium in the Earth I. Physical considerations. Phys. Earth Planet. Inter. 100, 61–79.
Kleine, T., Munker, C., Mezger, K., Palme, H., 2002. Rapid accretion and early core formation on asteroids and the terrestrial planets from Hf–W chronometry. Nature 418, 952–955.
Kojitani, H., Akaogi, M., 1997. Melting enthalpies of mantle peridotite: calorimetric determinations in the system CaO–MgO–Al_2O_3–SiO_2 and application to magma generation. Earth Planet. Sci. 153, 209–222.
Kurz, M.D., Jenkins, W.J., Hart, S.R., 1982. Helium isotopic systematics of oceanic islands and mantle heterogeneity. Nature 297, 43–47.
Labrosse, S., Poirier, J.P., Le Mouël, J.L., 1997. On cooling of the Earth's core. Phys. Earth Planet. Inter. 99, 1–17.
Labrosse, S., Hernlund, J.W., Coltice, N., 2007. A crystallizing dense magma ocean at the base of the Earth's mantle. Nature 450, 866–869.
Lauterbach, S., McCammon, C.A., van Aken, P., Langenhorst, F., Seifert, F., 2000. Mössbauer and ELNES spectroscopy of (Mg, Fe)(Si, Al)O3 perovskite: a highly oxidized component of the lower mantle. Contrib. Mineral. Petrol. 138, 17–26.

Please cite this article as: Andrault, D., et al., Solidus and liquidus profiles of chondritic mantle: Implication for melting of the Earth across its history, Earth Planet. Sci. Lett. (2011), doi:10.1016/j.epsl.2011.02.006

Lay, T., Williams, Q., Garnero, E.J., 1998. The core–mantle boundary layer and deep Earth dynamics. Nature 392, 461–468.
Lay, T., Garnero, E.J., Williams, Q., 2004. Partial melting in a thermo-chemical boundary layer at the base of the mantle. Phys. Earth Planet. Inter. 146, 441–467.
Li, J., Agee, C.B., 1996. Geochemistry of mantle–core differentiation at high pressure. Nature 381, 686–689.
Liebske, C., Corgne, A., Frost, D.J., Rubie, D.C., Wood, B.J., 2005. Compositional effects on element partitioning between Mg-silicate perovskite and silicate melts. Contrib. Mineral. Petrol. 149.
Litasov, K., Ohtani, E., 2002. Phase relations and melt compositions in CMAS–pyrolite–H_2O system up to 25 GPa. Phys. Earth Planet. Inter. 134, 105–127.
Luo, S.N., Akins, J.A., Ahrens, T.J., Asimow, P.D., 2004. Shock-compressed $MgSiO_3$ glass, enstatite, olivine, and quartz: optical emission, temperatures, and melting. J. Geophys. Res. Solid Earth 109.
Matas, J., Bass, J.D., Ricard, Y., Mattern, E., Bukowinsky, M.S., 2007. On the bulk composition of the lower mantle: predictions and limitations from generalized inversion of radial seismic profiles. Geophys. J. Int. 170, 764–780.
Mezouar, M., Crichton, W.A., Bauchau, S., Thurel, F., Witsch, H., Torrecillas, F., Blattmann, S., Marion, P., Dabin, Y., Chavanne, J., Hignette, O., Morawe, C., Borel, C., 2005. Development of a new state-of-the-art beamline optimized for monochromatic single-crystal and powder X-ray diffraction under extreme conditions at the ESRF. J. Synchrotron Radiat. 12, 559–664.
Miller, G.H., Stolper, E.M., Ahrens, T.J., 1991. The equation of state of a molten komatiite 2. Application to komatiite petrogenesis and the Hadean mantle. J. Geophys. Res. 96, 11,849–11,864.
Mosenfelder, J.L., Asimow, P.D., Frost, D.J., Rubie, D.C., Ahrens, T.J., 2009. The $MgSiO_3$ system at high pressure: thermodynamic properties of perovskite, postperovskite, and melt from global inversion of shock and static compression data. J. Geophys. Res. 114, B01203.
Murakami, M., Hirose, K., Kawamura, K., Sata, N., Ohishi, Y., 2004. Post-perovskite phase transition in $MgSiO_3$. Science 304, 855–858.
Nagahara, H., Ozawa, K., 1996. Evaporation of forsterite in H-2 gas. Geochim. Cosmochim. Acta 60, 1445–1459.
Nguyen, J.H., Holmes, N.C., 2004. Melting of iron at the physical conditions of the Earth's core. Nature 427, 339–342.
Nishio-Hamane, D., Seto, Y., Nagai, T., Fujino, K., 2007. Ferric iron and aluminum partitioning between $MgSiO_3$ and $CaSiO_3$ perovskites under oxydizing conditions. J. Mineral. Petrol. Sci. 102, 291–297.
Oganov, A.R., Ono, S., 2004. Theoretical and experimental evidence for a post-perovskite phase of $MgSiO_3$ in the Earth's D″ layer. Nature 430, 445–448.
Poirier, J.P., 1994. Light elements in the Earth's outer core: a critical review. Phys. Earth Planet. Inter. 85, 319–337.
Righter, K., Drake, M.J., Yaxley, G., 1997. Prediction of siderophile element metal–silicate partition coefficients to 20 GPa and 2800 °C: the effects of pressure, temperature, oxygen fugacity and silicate and metallic melt compositions. Phys. Earth Planet. Inter. 100, 115–134.
Ringwood, A.E., 1975. Pyrolite and the chondritic Earth model. In: GrawHill, M. (Ed.), International series in the Earth's and Planetary Sciences, pp. 189–194.
Rubie, D.C., Melosh, H.J., Reid, J.E., Liebske, C., Righter, K., 2003. Mechanism of metal–silicate equilibration in the terrestrial magma ocean. Earth Planet. Sci. 205, 239–255.
Rubie, D.C., Gessmann, C.K., Frost, D.J., 2004. Partitioning of oxygen during core formation on the Earth and Mars. Nature 429, 58–62.
Rudge, J.F., Kleine, T., Bourdon, B., 2010. Broad bounds on Earth's accretion and core formation constrained by geochemical models. Nat. Geosci. 3, 439–443.
Sata, N., Shen, G., Rivers, M.L., Sutton, S.R., 2002. Pressure–volume equation of state of the high-pressure B2 phase of NaCl. Phys. Rev. B 65, 114114–114117.
Shen, G., Prakapenka, V.B., Rivers, M.L., Sutton, S.R., 2004. Structure of liquid iron up to 58 GPa. Phys. Rev. Lett. 92, 185701.
Shim, S.H., Duffy, T.S., Shen, G., 2000. The equation of state of $CaSiO_3$ perovskite to 108 GPa at 300 K. Phys. Earth Planet. Inter. 120, 327–338.
Simon, F., Glatzel, G., 1929. Fusion–pressure curve. Z. Anorg. Allg. Chem. 178, 309–316.
Sleep, N.H., Zahnle, K.J., Neuhoff, P.S., 2001. Initiation of clement surface conditions on the earliest Earth. Proc. Natl. Acad. Sci. 98, 3666–3672.
Solomatov, V.S., 2000. Fluid dynamics of terrestrial magma ocean. In: Canup, R.M., Righter, K. (Eds.), Origin of the Earth and Moon. The University of Arizona Press, Tucson, Arizona, pp. 323–338.
Stacey, F.D., Davis, P.M., 2004. High pressure equations of state with applications to the lower mantle and core. Phys. Earth Planet. Inter. 142, 137–184.
Stevenson, D.J., 1990. Fluid dynamics of core formation. In: Newsom, H., Jones, J.H. (Eds.), The Origin of the Earth. Oxford Press, London, pp. 231–249.
Stixrude, L., Karki, B.B., 2005. Structure and freezing of $MgSiO_3$ liquid in the Earth's lower mantle. Science 310, 297–299.
Stixrude, L., de Koker, N., Sun, N., Mookherjee, M., Karki, B.B., 2009. Thermodynamics of silicate liquids in the deep Earth. Earth Planet. Sci. 278, 226–232.
Tateno, S., Hirose, K., Sata, N., Ohishi, Y., 2009. Determination of post-perovskite phase transition boundary up to 4400 K and implications for thermal structure in D″ layer. Earth Planet. Sci. 277, 130–136.
Tonks, W.B., Melosh, H.J., 1993. Magma ocean formation due to giant impacts. J. Geophys. Res-Planet 98, 5319–5333.
Tronnes, R.G., Frost, D.J., 2002. Peridotite melting and mineral–melt partitioning of major and minor elements at 22–24.5 GPa. Earth Planet. Sci. 197, 117–131.
Walker, D., Cranswick, L.M.D., Verma, P.K., Clark, S.M., Buhre, S., 2002. Thermal equations of state for B1 and B2 KCl. Am. Mineral. 87, 805–812.
Wasson, J.T., Kallemeyn, G.W., 1988. Composition of chondrites. Philos. Trans. R. Soc. Lond. A325, 535–544.
Wen, L., Helmberger, D.V., 1998. Ultra-low velocity zones near the core–mantle boundary from broadband PKP precursors. Science 279, 1701–1703.
Williams, Q., Jeanloz, R., Bass, J., Svendsen, B., Ahrens, T.J., 1987. The melting curve of iron to 250 GPa — a constraint on the temperature at earths center. Science 236, 181–182.
Wood, B.J., Walter, M.J., Wade, J., 2006. Accretion of the Earth and segregation of its core. Nature 441, 825–832.
Yamazaki, D., Kato, T., Ohtani, E., Toriumi, M., 1996. Grain growth rates of $MgSiO_3$ perovskite and periclase under lower mantle conditions. Science 274, 2052–2054.
Yoshino, T., Walter, M.J., Katsura, T., 2003. Core formation in planetesimals triggered by permeable flow. Nature 422, 154–157.
Zahnle, K.J., Kastings, J.F., Pollack, J.B., 1988. Evolution of a steam atmosphere during Earth's accretion. Icarus 74, 62–97.
Zerr, A., Diegeler, A., Boehler, R., 1998. Solidus of earth's mantle. Science 281, 243–246.

Please cite this article as: Andrault, D., et al., Solidus and liquidus profiles of chondritic mantle: Implication for melting of the Earth across its history, Earth Planet. Sci. Lett. (2011), doi:10.1016/j.epsl.2011.02.006